PCCP

Accepted Manuscript

ROYAL SOCIETY OF CHEMISTRY

www.rsc.org/pccp

Molecular simulations for dynamic nuclear polarization in liquids: A case study of TEMPOL in acetone and DMSO

Sami Emre Küçük,[a] Petr Neugebauer,[b] Thomas F. Prisner,[b] and Deniz Sezer[a*]

[a] *Faculty of Engineering and Natural Sciences, Sabancı University, Orhanlı-Tuzla, 34956 Istanbul, Turkey*

[b] *Institute of Physical and Theoretical Chemistry, Goethe University, Max-von-Laue Str. 7, 60438, Frankfurt am Main, Germany*

(Dated: January 17, 2015)

Abstract

A computational strategy for calibrating, validating and analyzing molecular dynamics (MD) simulations to predict dynamic nuclear polarization (DNP) coupling factors and relaxivities of proton spins is presented. Simulations of the polarizing agent TEMPOL in liquid acetone and DMSO are conducted at low (infinite dilution) and high (1 M) concentrations of the free radical. Because DNP coupling factors and relaxivities are sensitive to the time scales of the molecular motions, the MD simulations are calibrated to reproduce the bulk translational diffusion coefficients of the pure solvents. The simulations are then validated by comparing with experimental dielectric relaxation spectra, which report on the rotational dynamics of the molecular electric dipole moments. The analysis consists of calculating spectral density functions (SDFs) of the magnetic dipole-dipole interaction between the electron spin of TEMPOL and nuclear spins of the solvent protons. Here, MD simulations are used in combination with an analytically tractable model of molecular motion. While the former provide detailed information at relatively short spin-spin distances the latter includes contributions at large separations, all the way to infinity. The relaxivities calculated from the SDFs of acetone and DMSO are in excellent agreement with experiments at 9.2 T. For DMSO we calculate a coupling factor in agreement with experiment while for acetone we predict a value that is larger by almost 50%, suggesting possibility for experimental improvement.

I. INTRODUCTION

Over the last decade, the Overhauser effect[1] (OE) has received renewed attention as a means of increasing the NMR signal intensity in liquids at magnetic fields of interest for MRI and structural NMR.[2] The phenomenon, known as OE dynamic nuclear polarization (O-DNP), is well known,[3] but its observation at magnetic fields higher than ~ 3 T is recent.[4,5] Presently, high-field O-DNP measurements have been reported for protons of various liquids: water at 3.4 T[6–9] and 9.2 T,[10] toluene at 3.4 T[11] and 9.2 T,[12] ethanol at 3.4 T,[13] and acetone and DMSO at 9.2 T.[12]

Most of these studies not only report the O-DNP enhancement of the NMR signal but make an effort to explain its magnitude in terms of the molecular motions of the polarizing agent and the solvent.[10,12,13] In all such cases, the molecular dynamics is modeled as pure translational diffusion of hard spheres with the electron spin, S, and nuclear spin, I, located at the centers of their own spheres ("outer sphere" relaxation). Occasionally, additional rotational diffusion of a molecular complex with fixed separation between I and S ("inner sphere" relaxation) is introduced.[14] For both models the spectral density functions (SDFs) of the interaction between the electron and nuclear magnetic dipoles[15] are available analytically.[16–18]

While such simple models are probably a good starting approximation to the molecular motion in liquids, they clearly miss many subtleties like the off-centered location of the spins, the presence or absence of hydrogen bonding, hydrophobic interactions, methyl rotation, etc. These details are expected to be important for the fast ($\lesssim$ ps) relative dynamics between the nuclear and electron spins, which is the main source of O-DNP enhancement at high magnetic fields. In contrast to the idealized analytical models, fully atomistic molecular dynamics (MD) simulations account for all the geometric and energetic factors mentioned above. Therefore, for some time now, we have been advocating the calculation of the dipole-dipole SDF from MD simulations.[19]

In the approach we have developed MD simulations provide information about molecular motions as long as the molecules are not farther than several nanometers.[20] At larger intermolecular separations, where the precise molecular interactions and geometries are insignificant for small-molecule polarizing agents in simple liquids,[21] the contributions of the molecular motions to the dipolar SDF are calculated employing the analytical model of

translational diffusion.[17,18] The developed methodology has been successfully applied to the nitroxide radical TEMPOL in toluene[20] and in water.[22]

It should be stressed, however, that in spite of their richer detail compared to the model of translational diffusion of spherical particles MD simulations are also models, even if more complex. Depending on the employed energy force field (e.g., united or explicit atoms, with or without representation for lone pairs and atomic polarizability) the simulated properties of the examined liquid may be in fair or poor correspondence to reality. Even if not all liquid properties are manifested in the O-DNP phenomenon, for its quantitative prediction the simulations should correctly reflect not only the structure of the liquid around the polarizing agent but also the time scales on which this structure fluctuates and evolves. In fact, for a given energy force field, the static and dynamic liquid properties important for high-field O-DNP may be captured better for some liquids and worse for others. Therefore, for every different choice of solvent it is advisable to monitor some of the pure-liquid properties and validate them against experiments.

The purpose of the present paper is to provide guidelines for performing, validating and analyzing MD simulations with the aim of producing quantitative predictions that can be compared directly with high-field O-DNP experiments in simple liquids. The examples considered to this end are the spin polarization of acetone and DMSO protons by the free radical TEMPOL, for which measurements at 9.2 T were published recently.[12] A comparative study of these two liquids is particularly informative given their substantial structural similarity but very different dynamical properties. In addition, the two molecules—acetone and DMSO—nicely illustrate the effect of the employed force field on the examined liquid properties and predicted spin relaxation rates.

The object of main interest for proton O-DNP is the magnetic dipole-dipole SDF $J(\omega)$, which can be used to calculate the relaxation rates R_1^{II} and R_1^{IS}:[16,19]

$$R_1^{II} = k[3J(\omega_I) + 7J(\omega_S)], \quad R_1^{IS} = k5J(\omega_S). \tag{1}$$

These rates account for the contribution of the nuclear and electron spin polarizations (second superscript) to the nuclear (first superscript) T_1 as a result of the dipolar interaction between the two spins. In (1), ω_I and ω_S are the Larmor frequencies of the nuclear and electron spins. For $I = 1/2$ and $S = 1/2$ the proportionality coefficient is $k = (2\pi/5)(\hbar\gamma_S\gamma_I\mu_0/4\pi)^2 N_A C$, where γ_I and γ_S are the gyromagnetic ratios of the spins,

N_A is Avogadro's number, and C is the concentration of the paramagnetic species.

Both of the rates in (1) can be accessed experimentally. The former, by measuring the nuclear T_1 in the absence (T_1^0) and in the presence ($T_1^{\rm rad}$) of the radical:

$$R_1^{II} = 1/T_1^{\rm rad} - 1/T_1^0. \tag{2}$$

In O-DNP the dimensionless combination $f = R_1^{II} T_1^{\rm rad} = 1 - T_1^{\rm rad}/T_1^0$ is known as the leakage factor.[3] In nuclear magnetic relaxation dispersion (NMRD) measurements the ratio of R_1^{II} and the free radical concentration is known as the relaxivity:[14]

$$r = R_1^{II}/C. \tag{3}$$

Finally, the ratio of the two rates in (1) is the O-DNP coupling factor,

$$c = R_1^{IS}/R_1^{II}, \tag{4}$$

which can be determined experimentally from the relation $e = cfs\gamma_S/\gamma_I$ only if the enhancement of the NMR signal, e, and the extent of electron spin saturation, s, are measured separately (assuming f is already known). Thanks to the experimental access of the saturation achieved in Ref. 12, here we compare theoretical predictions of both R_1^{II} and c with experimental values for acetone and DMSO at 9.2 T.

In the next section we present our results. These are discussed in the broader context of O-DNP methodology in Sec. III. The paper ends with an outlook. The Supporting Information (SI) contains two sections: Methods and Additional Results. The former provides details about the simulations as well as their validation and analysis. The latter includes figures and tables that did not make it into the main text.

II. RESULTS

A. Liquid structure and dynamics: validation

The molecules of acetone and DMSO have similar structures (Fig. 1), containing the hydrogens to be polarized on methyl groups. However, while the heavy atoms of acetone are on a plane, they form a pyramid in DMSO due to the lone pair of electrons on the sulfur. According to the MD simulations of the pure solvents, the local structure of the two pure

liquids—as reflected by the radial distribution function (RDF) of the molecular centers of mass—is also similar (Fig. 2).

By design (see SI Methods), the translational diffusion coefficients in the simulations match the experimental values (Table 1). In addition to translation, the rotational diffusion of the solvent molecules is also expected to be important for high-field O-DNP, especially since it falls in the ps time window. Access to molecular orientations in liquids is readily gained by dielectric relaxation spectroscopy.[23,24] Therefore, to further assess the degree to which the simulated molecular dynamics of the pure solvents correspond to reality, we examined the frequency-dependent electric susceptibility of acetone and DMSO. The calculated ϵ'' (imaginary part of the relative permittivity) is compared with experiments in Fig. 3. The Debye (acetone) and Davidson-Cole (DMSO) fits to the experimental data[25,26] are shown with black dashed lines. Although the measurements for acetone extend up to 24 GHz, the analytical fit and our prediction are drawn till 100 GHz in order to visualize the position and amplitude of the peak. Unfortunately, the experiments for acetone are at 20°C[25] while our simulations are at 35°C. However, considering that the static dielectric constant of acetone drops only by 3 units when going from 25°C to 53°C, we expect the peak of ϵ'' at 35° to be about one unit lower than the one shown in Fig. 3 for 20°C. The position of the peak is also expected to be slightly shifted towards higher frequencies. The experimental data for DMSO are at 35°C and extend up to 26 GHz.[26]

From the results in Fig. 3 (red solid line) and the calculated static dielectric constant in Table 1, we conclude that the MD simulations of acetone overestimate the magnitude of ϵ by at most 10% and capture very well the time window where ϵ'' has a maximum. Thus, the time scales of orientation of the electric dipole moments of the acetone molecules in the simulated solution are realistic. The situation for the MD simulations performed with the CHARMM DMSO parameters[27] is drastically different. Here, the static dielectric constant is larger by almost 50% than the experimental value (Table 1).[28] Similarly, the peak of ϵ'' in Fig. 3 (blue solid line) is higher than experiment by about 60%. Furthermore, its position on the frequency axis is shifted to the left, indicating somewhat slower reorientation of the electric dipoles of DMSO in the simulated solution compared to reality.

In an effort to address this discrepancy we changed the partial charges of the heavy atoms of DMSO retaining all the other parameters. It should be stressed, however, that developing a new DMSO model for MD simulations is not our objective. Therefore, when modifying the

DMSO partial charges we limited ourselves to charges existing in the literature. The choice we consider and refer to as DMSO* is from Ref. 29. The partial charges of the simulated solvents are compiled in Table 2. The last column of the table reveals that the electric dipole moment of the modified model, DMSO*, is smaller than DMSO. For the pure liquid, this leads to a lower static dielectric constant (Table 1) and ϵ'' closer to experiment (Fig. 3, -·- cyan line). In the case of the latter, not only the amplitude of the peak but its position on the frequency axis as well have improved. From the point of view of dielectric response, the overall deviation of DMSO* from experiment is seen to be about 20-25%, which is half of the deviation of DMSO.

With this knowledge about the dynamic properties of the simulated pure liquids we now proceed to the simulations with doped TEMPOL.

B. Liquid properties in the presence of TEMPOL

Two different sets of simulations were performed for each solvent: the first, containing one TEMPOL molecule in the simulation box, the second, containing 1 M TEMPOL (see SI Methods). The simulations with one TEMPOL reveal that the solvent structure around the "impurity" is also very similar for the two solvents (Fig. 4a). For both solvents, the maxima and minima in density are found to occur at identical distances from the polarizing agent, with DMSO exhibiting somewhat larger amplitude of oscillations compared to acetone. (Almost identical RDFs are obtained for DMSO and DMSO*.) The RDFs are seen to flatten only beyond about 2 nm from TEMPOL.

In Sec. II C, where dipole-dipole SDF is calculated by dividing the space around TEMPOL into near and far regions, couplings to solvent spins beyond $d = 2.5$ nm are accounted for analytically using the model of hard spheres with centered spins (HSCS).[17,18] Although the contribution of distant dipoles to the SDF is not very sensitive to the model parameter referred to as the "distance of closest approach," we choose the values of b to be the distance at which the RDFs are equal to 0.5 (first three rows of Table 4).

Previously, for 1 M TEMPOL in water, we found that the TEMPOL molecules tend to form nanoclusters, from which the solvent is substantially excluded.[22] It is therefore of interest to determine whether the polarizing agent is well accessed by acetone and DMSO when present at high concentration. The TEMPOL-solvent RDFs calculated from the MD

simulations with 1 M TEMPOL (Fig. 4b) are very similar to those shown in Fig. 4a, demonstrating that solvent molecules access the polarizing agent as much as in the dilute case. A further check on cluster formation is provided by the TEMPOL-TEMPOL RDFs in the two solvents, which are shown in SI Fig. S1. Constant TEMPOL density is seen to be established in acetone and DMSO* beyond about 2 nm from any given TEMPOL molecule. Surprisingly, in DMSO (but not DMSO*) the free radicals show a tendency to stay closer together (without forming clusters from which the solvent is excluded). The absence of cluster formation is essential for the applicability of the analysis in the following sections.

The coefficients of translational diffusion of the solvent and the polarizing agent determined from the two sets of MD simulations are compiled in Table 3. When only one TEMPOL molecule is introduced in the simulation box the solvent diffusion (first column of Table 3) remains practically unchanged from its bulk value (Table 1). As expected, the diffusion of the single TEMPOL in acetone is faster than its diffusion in DMSO (third column of Table 3). In fact, the ratio of the MD diffusion coefficients is close to the ratio of the solvent viscosities. However, scaling the diffusion coefficient of TEMPOL in water (0.5 nm^2/ns at 35°C[22]) by the viscosities of the solvents predicts slower translational diffusion in both acetone and DMSO (1.27 nm^2/ns and 0.22 nm^2/ns) compared to the MD values in Table 3, indicating that the diffusion of TEMPOL in water is different in nature than its diffusion in acetone and DMSO.[30]

The 1 M TEMPOL simulations of acetone and DMSO demonstrate that both the solvent and TEMPOL molecules are slower at the elevated solute concentration (1 M columns of Table 3). Surprisingly, the opposite trend is observed for the simulation with DMSO*. Here, both the solvent and TEMPOL molecules appear to be faster at the elevated TEMPOL concentration. This qualitative difference between the two DMSO parameter sets can be traced back to differences in the predicted density of the 1 M mixture, for which experimental data are not available. (For the volume at which the 1M TEMPOL simulations are performed see SI Methods).

By adding the solvent and TEMPOL diffusion coefficients from Table 3, an estimate of the translational coefficient for relative solvent-TEMPOL motion can be obtained. These values, given in the first three rows of Table 4, are used in the calculation of the dipolar SDF in Sec. II C. In Sec. II D it is found that the relaxivities and O-DNP coupling factors calculated for low and high radical concentrations reflect the differences in the translational

dynamics of the molecules observed in the MD simulations.

How about the rotational dynamics of the molecules? The solvent dielectric response from the simulations with one TEMPOL is essentially identical to that of pure solutions (data not shown). In the case of a mixture the absorption can be written as $\epsilon'' = \epsilon''_{\mathrm{SS}} + \epsilon''_{\mathrm{ST}} + \epsilon''_{\mathrm{TT}}$, where the subscripts denote solvent-solvent (SS), solvent-TEMPOL (ST), and TEMPOL-TEMPOL (TT) contributions (see SI Methods). The dielectric response spectra calculated from the simulations of acetone and DMSO with 1 M TEMPOL are shown in Fig. 5. Comparing the profiles of ϵ'' with those for pure solvents (Fig. 3) we see that in all cases the magnitude of the peak has decreased by about 30%. For acetone and DMSO, the position of the peak on the frequency axis remains practically unchanged. In other words, the time scales of rotational diffusion of the solvent molecules do not seem to be affected by the presence of 1 M TEMPOL. In contrast, the peak of DMSO* in Fig. 5b (−·− cyan line) has shifted to higher frequencies compared to the pure solvent (Fig. 3). In Sec. II D we find that this shift to faster time scales at elevated TEMPOL concentration leads to predicted DNP coupling factors which are larger than the for dilute case.

C. Dipolar spectral densities

Magnetic dipole-dipole time correlation functions (TCFs) are calculated from the MD simulations and Fourier transformed to obtain the corresponding SDFs. In the calculation, the space around a given TEMPOL radical is imagined to be composed of a near region (N) and a far region (F), as depicted schematically in Fig. 6. Because the TCF $C(t)$ depends on the dipolar coupling at two instances in time separated by t, four possibilities arise for a given solvent molecule: it is in N at both times (Fig. 6, black path), it is in F at both times (gray path), it has moved from N to F (green path), and it has moved from F to N. The last two possibilities contribute equally to the TCF. Furthermore, in the analysis of the MD simulations solvent molecules farther than a distance a from TEMPOL (dashed circle) are assumed to disappear. The value of this cut-off distance is dictated by the size of the simulation box.

The C_{NN} and C_{NF} contributions to the TCFs calculated from the MD simulations with 1 TEMPOL are given in Figs. 7a and 7b, respectively. The solid lines are calculated by taking the nuclear spin to be at the position of a proton, and the electron spin to be divided equally

between the TEMPOL nitrogen and oxygen atoms. The dashed lines, on the other hand, are calculated from the same MD trajectories but pretending that the spins are located at the centers of mass (COM) of the molecules. Clearly, the exact position of the spins is inconsequential once their separation is larger than our choice of $d = 2.5$ nm (Fig. 7b). In contrast, for shorter separations, the locations of the spins on the molecules influence C_{NN} (Fig. 7a). The difference is dramatic at shorter times, which are of particular importance for O-DNP at high magnetic fields.

In the MD simulations the far region extends up to the edge of the simulation box, which typically is a few nanometers. To correct for its finite size, the far-far contribution to the SDF, $J_{\mathrm{FF}}(\omega)$, is calculated using the HSCS model.[21] Analytical finite-size corrections to $J_{\mathrm{NF}}(\omega)$ and $J_{\mathrm{NN}}(\omega)$ are obtained by calculating the difference between the HSCS model and its finite-size version with absorbing outer boundary.[20,22] All these corrections, however, assume that the approximations of hard spherical molecules with spins at their centers hold for sufficiently large inter-spin separations.

To validate these approximations, SDFs obtained by Fourier transforming the COM TCFs from Fig. 7 are fitted by the finite-size HSCS model. The best fits, shown in Fig. 8, demonstrate that the analytical model reproduces the SDFs from the MD simulations rather well. In light of Fig. 7b, the fit in Fig. 8b implies that for solvent molecules starting in the near region and reaching the far region the HSCS model is able to reproduce J_{NF} with reasonable values of the model parameters b and D (middle of Table 4). However, as with toluene[20] and water,[22] we find that the best-fit parameter D is smaller than the sum of the coefficients of translational diffusion of the TEMPOL and solvent molecules (first three rows of Table 4). In the case of J_{NN}, the agreement in Fig. 8a is with the calculations where the spins are taken to be at the COM of the molecules, which is one of the approximations of the HSCS model.[31] In this case the best fitting D is even smaller (last three rows of Table 4), as observed previously.[20,22]

The same analysis was performed for the simulations with 1 M TEMPOL. The TCFs are shown in SI Fig. S2. As expected from the faster dynamics in DMSO* compared to DMSO, substantial differences are visible between the two parameter sets (inset of SI Fig. S2b). Fits to the Fourier transforms of the TCFs are given in SI Fig. S3 while their parameters are compiled in Table 4.

The analytical fits to the SDFs calculated from the MD simulations are used to calcu-

late finite-size corrections, Δ^{fs}, as described in our previous work.[20,22] Putting everything together, the dipolar SDF is calculated as

$$J = (J^{\mathrm{MD}}_{\mathrm{NN}} + \Delta^{\mathrm{fs}}_{\mathrm{NN}}) + 2(J^{\mathrm{MD}}_{\mathrm{NF}} + \Delta^{\mathrm{fs}}_{\mathrm{NF}}) + J^{\mathrm{HSCS}}_{\mathrm{FF}}, \tag{5}$$

where the superscripts indicate where each J comes from. The three additive contributions on the right-hand side of the equality in (5) and the total dipolar SDF are plotted as a function of frequency in Fig. 9 for the dilute and in SI Fig. S4 for the concentrated TEMPOL solutions. Because of the relatively large size of the near region ($d = 2.5$ nm) most of the contribution to the SDF comes from the near-near (NN) correlation function. With the further choice of absorbing boundary at $a = 3.4$ nm, the near-far (NF) and far-far (FF) contributions end up being comparable in magnitude.

As evident from (1), in an experiment at a given magnetic field the relaxivity (3) and the DNP coupling factor (4) probe only two values of the dipolar SDF, $J(\omega_I)$ and $J(\omega_S)$. These are indicated with symbols in Fig. 9 and SI Fig. S4 for two different choices of the magnetic field—0.33 T (blue) and 9.2 T (red)—both of which have received considerable experimental attention in the last five years. At the electron Larmor frequency the NN contribution completely dominates the SDF for both magnetic fields (triangles). At the proton Larmor frequency, however, the finite-size corrections to MD become important for the quantitative determination of the SDF (circles), especially at the lower field of 0.33 T.

D. Relaxivity and coupling factors

Armed with the dipolar SDFs we proceed to calculate the relaxivity according to (3) and (1). To this end, one copy of the SDF is multiplied by 3, while another copy is multiplied by 7 and shifted to the left along the frequency axis until the same-colored symbols in Fig. 9 are aligned. Finally these two contributions are added together and scaled appropriately. Figure 10 shows the two added parts (dashed lines) and their sum (solid line) for the dilute TEMPOL solutions of acetone and DMSO. At 0.33 T (15 MHz/9.7 GHz) $3J(\omega_I)$ and $7J(\omega_S)$ contribute equally to the relaxivity in acetone (Fig. 10a, blue symbols). In the case of DMSO, $7J(\omega_S)$ is about one fourth of $3J(\omega_I)$ (Fig. 10b, blue symbols). The relaxivity measurement at this field, therefore, encodes information about the dipolar SDF at both the nuclear and electron Larmor frequencies. In contrast, the relaxivity at 9.2 T (400 MHz/260 GHz) is

dominated by the contribution of $3J(\omega_I)$ for both acetone and DMSO (Fig. 10, red symbols). There is little hope, therefore, of accessing $7J(\omega_S)$ on the background of $3J(\omega_I)$ from measurements of the relaxivity at high magnetic fields. The ability to separate these two contributions is essential for predicting DNP coupling factors from NMRD relaxivity measurements.

Our predictions of the relaxivity in Fig. 10 (solid lines) are compared with published[12] NMRD values (diamonds). The agreement at 260 GHz is very good. At and around 10 GHz, our predicted values for acetone are smaller than the NMRD measurements (Fig. 10a). The agreement is better for DMSO, where our values are somewhat larger (Fig. 10b). The same analysis was performed for the MD simulations with 1 M TEMPOL (plots not shown).

The NMRD measurements that we compare with were performed with 40 mM TEMPOL solutions.[12] To assess the extent of variation of the relaxivity due to the experimental uncertainty in the concentration of the polarizing agent, in Fig. 11 we report the relaxivities deduced from nuclear T_1 measurements of solutions with different TEMPOL concentrations and at different temperatures. (The T_1 values are given in SI Table S1.) For acetone (Fig. 11a), the temperature variation of the relaxivity is seen to be smaller than the variation due to the TEMPOL concentration. The NMRD value at 35°C (black diamond) agrees very well with the other measurements. Similarly, the relaxivities computed from the MD simulations with 1 TEMPOL (black star at 2 mM) and 1 M TEMPOL (black star at 1000 mM) are in very good agreement with the experimental data.

The situation is different for DMSO (Fig. 11b). Here, the variation of the relaxivity with the concentration of TEMPOL is smaller than its change due to temperature. A small decrease of the relaxivity is measured at the largest two TEMPOL concentrations of 500 mM and 1 M. The NMRD value at 35°C (diamond) is closer to the experimental values at 39°C, whereas the relaxivities calculated from the MD simulations of DMSO (star) and DMSO* (asterisk) containing 1 TEMPOL are somewhat larger than the values at 39°C, in perfect agreement with what should be expected at 35°C. The MD calculations for 1 M TEMPOL differ between DMSO and DMSO*. The former model predicts larger relaxivity, comparable with the experimental values for lower TEMPOL concentrations at 22°C. This increase in the relaxivity with increase in the TEMPOL concentration is due to the decreasing coefficient of relative translational diffusion in the MD simulations (Table 4). The relaxivity calculated from the DMSO* simulations, on the other hand, agrees with what is expected from the low

concentration measurements at 39°C. None of the models, however, captures the decrease of the relaxivity at TEMPOL concentrations above 0.5 M that is seen in the experiment.

Having tested the ability of the calculated SDFs to predict the relaxivity, we now use them to compute DNP coupling factors for several different magnetic fields spanning the range of experimental interest (Table 5). As expected on the basis of the viscosities of the two solvents, the coupling factors of acetone are larger than DMSO. From a methodological point of view, it is encouraging that the coupling factors for the dilute DMSO solutions (before the slash) predicted by the two models—DMSO and DMSO*—are very similar. In line with the reduction of the diffusion coefficients (Table 3), smaller coupling factors are predicted for acetone and DMSO at the higher TEMPOL concentration. In contrast, again as expected from the diffusion coefficients, the simulations with DMSO* predict larger coupling factors at 1 M TEMPOL. In Fig. 12 the 1 M TEMPOL values at 260 GHz are compared with experiment.[12] While both DMSO and DMSO* agree well with the measurements (Fig. 12b), the latter is seen to perform better. In contrast, the coupling factor of acetone in our simulations is almost 50% larger than experiment (Fig. 12a). This is in spite of the excellent agreement of the computed relaxivity with measurements (Fig. 11a), demonstrating that very similar values of the relaxivity can correspond to drastically different coupling factors, in line with the observations of Ref. 12.

III. DISCUSSION

A computational strategy for calibrating, validating, and analyzing MD simulations with the purpose of predicting proton DNP coupling factors and relaxivities at high (> 3 T) magnetic fields was presented. The methodology was illustrated for acetone and DMSO solutions doped with the polarizing agent TEMPOL. In the simulations TEMPOL was present at either infinite dilution or at a concentration of 1 M. Although experimental information about the physical properties of the solvent-TEMPOL mixtures at elevated radical concentration is missing, these simulations were necessary for the direct comparison with experimentally determined DNP coupling factors at 9.2 T.

Due to the sensitivity of the relaxivity and DNP coupling factors to molecular motions, at the calibration stage of the procedure it was essential to know the coefficient of translational diffusion of the solvent, as already made clear in our previous work.[19,20,22] Here, in addition,

we employed data from dielectric relaxation spectroscopy to validate the MD simulations in terms of the rotational motion of the solvent molecules. Deficiencies in the force field parameters used to simulate the dynamics of the molecules may become apparent at this stage, as was the case for DMSO. The considered DMSO model with reduced partial charges (Table 2) that we called DMSO* agreed better with dielectric response experiment (Fig. 3). However, it should be emphasized that we have not attempted to illustrate a general strategy for reparametrization of the molecular model, since this is a step that requires a separate, full-blown effort.

Recently, dielectric response and its relevance in the quantitative analysis of O-DNP data has been discussed in Ref. 32. Observing that liquid-state DNP experiments are typically performed under constant microwave irradiation, the authors examined the variation of the nuclear T_1 of water with microwave power and related it to the (undesired) coupling of the water electric dipoles to the electric field component of the microwaves.[32] While the irreversible dipole orientations (reflected by ϵ'') can be compensated by active cooling, it has been pointed out that the adiabatic dipole orientations induced by the microwaves (reflected by ϵ') lead to additional molecular motions, which change the nuclear T_1 and could also influence the O-DNP coupling factor.

It has been shown, however, that under DNP conditions the microwave influence on nuclear T_1 is an issue only when the concentration of the polarizing agent is less than about 100 mM.[32] Because the coupling factors we compared with are deduced from samples with 1 M TEMPOL (Fig. 12), proton T_1 is dominated by the radical concentration. Furthermore, since ϵ' drops sharply in the frequency window corresponding to the peak of ϵ'' (Figs. 3 and 5), while ϵ' is substantial for both acetone and DMSO at 10 GHz, the frequency examined in Ref. 32, it is negligibly small at 260 GHz. Thus, the complications for samples with low radical concentration measured at X-band are not an issue in our case.

Once calibrated and validated, the MD simulations were used to calculate the spectral density function (SDF) of the magnetic dipole-dipole coupling of the electron and nuclear spins. At this stage, the main strength of our procedure is the combined use of MD simulations and analytical calculations. While the former are rich in structural and motional details they are limited in size. In contrast, analytical models effortlessly extend to infinite distances but rely on drastic simplifications of molecular structures and dynamics. The synergistic use of these computational techniques in the regimes of their respective applicabilities has

been proposed in Ref. 21 and further developed in Refs. 20 and 22.

Naturally, this methodology has its own range of applicability: At distances sufficiently far from the polarizing agent but still accessible to MD simulations all the simplifying approximations of the analytical HSCS model should apply. By fitting the near-far SDF obtained from the MD simulations to the finite-size version of the HSCS model (Fig. 8b and SI Fig. S3b) we made sure that such an approximate description is indeed possible once the solvent molecules have moved to distances larger than $d = 2.5$ nm from TEMPOL. This justified the analytical calculation of the far-far SDF using the HSCS model and its inclusion according to (5). Appealing to the HSCS model at sufficiently large distances limits the application of the present methodology to homogeneous, spherically isotropic systems of small-molecule solvents and radicals. It was, therefore, essential to establish that at a concentration of 1 M the TEMPOL molecules are still homogeneously dispersed in acetone and DMSO (Fig. 4b and SI Fig. S1). Because several force-field parameters (e.g., Lennard-Jones, partial atomic charges) conspire to determine whether the two components of a mixture will stay well mixed or will form nanoscopic clusters, the outcome is not easily predictable, especially in the case of nitroxides, which are amphiphilic.

The SDFs from the dilute and 1 M TEMPOL simulations were used to calculate proton relaxivities and DNP coupling factors at 9.2 T (Figs. 11 and 12), where direct comparison with experiments was possible. While the relaxivities for both acetone and DMSO (especially DMSO*) were in excellent agreement with experiments, only the coupling factor of DMSO (especially DMSO*) matched the measurements. Clearly, motional models that agree with the relaxivity need not be in agreement with the coupling factor, as has been demonstrated in Ref. 12. From Fig. 10, which shows the relative contributions of $3J(\omega_I)$ and $7J(\omega_S)$ to R_1^{II}, the poor link between the relaxivity and coupling factor is expected to be the rule at high fields.

For acetone, the calculated coupling factor at 1 M was almost 50% larger than the experimental value (Fig. 12a). This discrepancy could be an indication that the physical properties of the simulated acetone-TEMPOL mixture are flawed, in spite of the very good dynamical behavior of the pure acetone solution, reflected by its dielectric absorption spectrum (Fig. 3). On the other hand, if the computational prediction is taken seriously, the disagreement between theory and experiment could be an indication that spin interactions that are not accounted for in the analysis are actually operational. For example, additional scalar coupling

between the electron and proton spins will tend to reduce the coupling factor due to pure dipolar interaction. Although it is not clear why such hypothetical scalar coupling does not occur for DMSO protons, one could envision performing *ab initio* calculations using the MD snapshots to quantify the magnitude of the Fermi contact between the unpaired electron and the acetone protons. The most optimistic possibility, of course, is that future improvements in the experimental setup at 260 GHz could indeed lead to a measured DNP coupling factor in agreement with the computational prediction for 1 M TEMPOL in acetone. This would imply enhancements that are almost 50% larger than what has been achieved so far. According to our calculations (Table 5), even larger acetone enhancement should be possible at lower TEMPOL concentrations in case the electron spin saturation at 260 GHz is not compromised.

IV. OUTLOOK

In conclusion, the presented methodology is now sufficiently developed to be directly employed to compare with O-DNP and T_1 relaxivity measurements of nitroxide radicals in simple liquids at intermediate ($\geq$ 0.3 T) and high ($>$ 3 T) magnetic fields. It is especially powerful in illuminating subtle differences between different types of protons on the same molecule (e.g., ring and methyl protons of toluene,[11,12,33] or methyl, methylene and hydroxyl protons of ethanol[13]) or between same type of protons on structurally similar molecules (e.g., methyl protons of acetone and DMSO).

In the present study, whose main focus was high-field O-DNP, calculation of dielectric response spectra from MD simulations was employed as a tool for validating the rotational dynamics of the solvent molecules. In future work it should be possible to employ the calculated dispersion relation of ϵ' to estimate the magnitude of the adiabatic rotational motion induced by the electric field of the microwaves and to quantify its contribution to both the nuclear T_1 and the coupling factor at X-band, thus critically assessing the magnitude of the effects proposed in Ref. 32.

The combined use of MD simulations in the near region with analytical treatment in the far region, should also be directly applicable to the calculation of intermolecular nuclear Overhausser effect (NOE) in liquids. The structure and dynamics of ionic liquids, for example, is extensively probed with MD simulations.[34,35] While dielectric spectroscopic relaxation

has been the experimental technique of choice to compare such studies with,[36] intermolecular NOE has also received attention.[37] However, when comparing dipole-dipole SDFs from MD simulations of ionic liquids with analytical expressions, the possibility that the observed discrepancies could be due to the finite size of the simulation box is often neglected.[37] As should be clear from Fig. 9, the SDF at the nuclear Larmor frequencies, which are of relevance in NOE experiments, is especially sensitive to the size of the atomistic region, in agreement with the long-ranged nature of NOE interactions known from the literature.[38]

The HSCS model, which is used in combination with the MD simulations, assumes a homogeneous and rotationally isotropic environment. Unfortunately, this prevents the direct application of the methodology to spin-labeled biological macromolecules, i.e., proteins, DNA and RNA, as well as to heterogeneous environments, like lipid micelles and bilayers, which have been studied with O-DNP in the last few years.[32,39,40] We are currently exploring avenues of extending the outlined methodology to these more challenging settings.

ACKNOWLEDGMENTS

S.E.K. is a recipient of a TUBITAK-BIDEP graduate scholarship. This work is supported by TUBITAK Career Grant No. 112T770 (D.S.) and Deutsch-Israelische Projektkooperation DFG grant (T.F.P.). The stimulating interaction environment of the COST action TD1103 on Hyperpolarization Physics and Methodology in NMR and MRI is gratefully acknowledged.

---

* dsezer@sabanciuniv.edu

[1] A. W. Overhauser, Phys. Rev. **92**, 411 (1953).

[2] C. Griesinger, M. Bennati, H. M. Vieth, C. Luchinat, G. Parigi, P. Höfer, F. Engelke, S. J. Glaser, V. Denysenkov, and T. F. Prisner, Prog. Nucl. Magn. Reson. Spectrosc. **64**, 4 (2012).

[3] K. H. Hausser and D. Stehlik, Adv. Magn. Reson. **3**, 79 (1968).

[4] P. Höfer, G. Parigi, C. Luchinat, P. Carl, G. Guthausen, M. Reese, T. Carlomagno, C. Griesinger, and M. Bennati, J. Am. Chem. Soc. **130**, 3254 (2008).

[5] M. J. Prandolini, V. P. Denysenkov, M. Gafurov, B. Endeward, and T. F. Prisner, J. Am. Chem. Soc. **131**, 6090 (2009).

[6] M.-T. Türke, I. Tkach, M. Reese, P. Höfer, and M. Bennati, Phys. Chem. Chem. Phys. **12**, 5893 (2010).

[7] E. V. Kryukov, K. J. Pike, T. K. Y. Tam, M. E. Newton, M. E. Smith, and R. Dupree, Phys. Chem. Chem. Phys. **13**, 4372 (2011).

[8] P. J. M. van Bentum, G. H. A. van der Heijden, J. A. Villanueva-Garibay, and A. P. M. Kentgens, Phys. Chem. Chem. Phys. **13**, 17831 (2011).

[9] M. T. Türke and M. Bennati, Appl. Magn. Reson. **43**, 129 (2012).

[10] P. Neugebauer, J. G. Krummenacker, V. P. Denysenkov, G. Parigi, C. Luchinat, and T. F. Prisner, Phys. Chem. Chem. Phys. **15**, 6049 (2013).

[11] E. V. Kryukov, M. E. Newton, K. J. Pike, D. R. Bolton, R. M. Kowalczyk, A. P. Howes, M. E. Smith, and R. Dupree, Phys. Chem. Chem. Phys. **12**, 5757 (2010).

[12] P. Neugebauer, J. G. Krummenacker, V. P. Denysenkov, C. Helmling, C. Luchinat, G. Parigi, and T. F. Prisner, Phys. Chem. Chem. Phys. **16**, 18781 (2014).

[13] G. H. A. van der Heijden, A. P. M. Kentgens, and P. J. M. van Bentum, Phys. Chem. Chem. Phys. **16**, 8493 (2014).

[14] M. Bennati, C. Luchinat, G. Parigi, and M.-T. Türke, Phys. Chem. Chem. Phys. **12**, 5902 (2010).

[15] For protons the dipolar interaction between the electron and nuclear spins appears to be responsible for the O-DNP effect. In contrast, when carbon nuclear spins are polarized the scalar coupling is also operative.

[16] A. Abragam, *The Principles of Nuclear Magnetism* (Oxford University Press, New York, 1961).

[17] Y. Ayant, E. Belorizky, J. Alizon, and J. Gallice, J. Phys. (Paris) **36**, 991 (1975).

[18] L.-P. Hwang and J. H. Freed, J. Chem. Phys. **63**, 4017 (1975).

[19] D. Sezer, M. J. Prandolini, and T. F. Prisner, Phys. Chem. Chem. Phys. **11**, 6626 (2009).

[20] D. Sezer, Phys. Chem. Chem. Phys. **15**, 526 (2013).

[21] P. H. Fries, D. Imbert, and A. Melchior, J. Chem. Phys. **132**, 044502 (2010).

[22] D. Sezer, Phys. Chem. Chem. Phys. **16**, 1022 (2014).

[23] C. J. F. Böttcher and P. Bordewijk, *Theory of Electric Polarization*, 2nd ed., Vol. II: Dielectrics in Time-Dependent Fields (Elsevier Science B. V., 1978).

[24] S. Gekle and R. R. Netz, J. Chem. Phys. **137**, 104704 (2012).

[25] J. Barthel and R. Buchner, Pure & Appl. Chem. **63**, 1473 (1991).

[26] Z. Lu, E. Manias, D. D. Macdonald, and M. Lanagan, J. Phys. Chem. A **113**, 12207 (2009).

[27] M. L. Strader and S. E. Feller, J. Phys. Chem. A **106**, 1074 (2002).

[28] The static ϵ is calculated in Ref. 27 from MD simulations at 30°C and reported to be 40.4, which is smaller than experiment by less than 15%. In our hands, ϵ is larger than experiment by almost 50%. The origin of this discrepancy is not clear to us.

[29] P. Bordat, J. Sacristan, D. Reith, S. Girard, A. Glättli, and F. Müller-Plathe, Chem. Phys. Lett. **374**, 201 (2003).

[30] The viscosities of acetone, water and DMSO at 35°C are 0.283 mPa s, 0.719 mPa s and 1.655 mPa s, respectively.

[31] This point is further examined at the end of SI Sec. II D. See Figs. S5 and S6 in particular.

[32] J. M. Franck, A. Pavlova, J. A. Scott, and S. Han, Prog. Nucl. Magn. Reson. Spectrosc. **74**, 33 (2013).

[33] N. Enkin, G. Liu, I. Tkach, and M. Bennati, Phys. Chem. Chem. Phys. **16**, 8795 (2014).

[34] C. Schröder and O. Steinhauser, J. Chem. Phys. **133**, 154511 (2010).

[35] S. Gabl, C. Schröder, and O. Steinhauser, J. Chem. Phys. **137**, 094501 (2012).

[36] C. Schröder and O. Steinhauser, J. Chem. Phys. **132**, 244109 (2010).

[37] S. Gabl, C. Schröder, D. Braun, H. Weingärtner, and O. Steinhauser, J. Chem. Phys. **140**, 184503 (2014).

[38] B. Halle, J. Chem. Phys. **119**, 12373 (2003).

[39] C.-Y. Cheng and S. Han, Annu. Rev. Phys. Chem. **64**, 507 (2013).

[40] J. Song, J. Franck, P. Pincus, M. W. Kim, and S. Han, J. Am. Chem. Soc. **136**, 2642 (2014).

[41] H. Ertl and F. A. L. Dullien, AIChE Journal **19**, 1215 (1973).

[42] M. Holz, S. R. Heil, and A. Sacco, Phys. Chem. Chem. Phys. **2**, 4740 (2000).

[43] K. Vanommeslaeghe, E. Hatcher, C. Acharya, S. Kundu, S. Zhong, J. Shim, E. Darian, O. Guvench, P. Lopes, I. Vorobyov, and A. D. Mackerell, J. Comput. Chem. **31**, 671 (2010).

[44] D. Sezer, J. H. Freed, and B. Roux, J. Phys. Chem. B **112**, 5755 (2008).

[45] J. C. Phillips, R. Braun, W. Wang, J. Gumbart, E. Tajkorshid, E. Villa, C. Chipot, R. D. Skeel, L. Kale, and K. Schulten, J. Comp. Chem. **26**, 1781 (2005).

TABLE 1. Liquid properties calculated from MD simulations at 35°C with the given choice of thermostat damping (γ): coefficients of translational diffusion (D) and static dielectric constants (ϵ). (One standard deviation in parenthesis.)

	γ/ps^{-1}	$D/\mathrm{nm}^2\mathrm{ns}^{-1}$[a]	ϵ[b]
Acetone	0.015	5.09 (0.37)	21.4 (0.7)
DMSO	0.072	0.94 (0.20)	68.1 (0.5)
DMSO*	0.050	0.92 (0.03)	54.3 (3.6)

[a] Targeted experimental values (35°C): $D = 5.19$ nm^2/ns (acetone),[41] $D = 0.889$ nm^2/ns (DMSO).[42]
[b] Experiment: $\epsilon = 20.6$ (acetone, 20°C),[25] $\epsilon = 46.6$ (DMSO, 35°C).[26]

TABLE 2. Partial charges (atomic units) of the specified atoms and the resulting molecular dipole moments (Debye).

	O	C/S	C	H	μ^{a}
Acetone	−0.480	0.400	−0.230	0.09	3.6
DMSO	−0.556	0.312	−0.148	0.09	5.2
DMSO*	−0.437	0.117	−0.110	0.09	4.8

[a] Gas phase: $\mu = 2.9$ D (acetone), $\mu = 4.0$ D (DMSO).

TABLE 3. Diffusion coefficients (nm^2/ns) calculated from the simulations with one TEMPOL (1), or 1 M TEMPOL (1 M). (One standard deviation in parenthesis.)

	solvent		TEMPOL	
	1	1 M	1	1 M
Acetone	4.93 (0.22)	4.54 (0.37)	3.18 (0.42)	2.66 (0.34)
DMSO	0.88 (0.01)	0.73 (0.03)	0.60 (0.02)	0.41 (0.01)
DMSO*	0.98 (0.01)	1.08 (0.08)	0.61 (0.09)	0.67 (0.04)

TABLE 4. Values of b (nm) and D (nm^2/ns) determined from the fits to the MD SDFs with the finite-size HSCS model.[20] Numbers before and after the slash are for the simulations with 1 TEMPOL and 1 M TEMPOL, respectively.

	solvent	b	D
J_{FF}	Acetone	0.51/0.55	8.11/7.20
	DMSO	0.51/0.55	1.48/1.14
	DMSO*	0.51/0.51	1.59/1.75
J_{NF}	Acetone	0.40/0.45	6.16/5.20
	DMSO	0.45/0.47	1.16/0.93
	DMSO*	0.45/0.45	1.15/1.25
J_{NN}	Acetone	0.45/0.45	5.22/4.10
	DMSO	0.45/0.43	0.96/0.81
	DMSO*	0.45/0.43	0.88/1.07

TABLE 5. Coupling factors (%) at the specified ESR(NMR) frequencies (GHz/MHz) computed from the simulations with 1 TEMPOL (before the slash) and 1 M TEMPOL (after the slash).

	9.7(15)	34(50)	94(140)	260(400)	460(700)
Acetone	36.3/33.6	20.0/16.9	9.41/7.70	3.50/2.90	2.05/1.75
DMSO	13.4/10.3	4.88/3.60	1.53/1.15	0.69/0.56	0.44/0.38
DMSO*	13.1/13.9	4.79/5.28	1.50/1.71	0.65/0.74	0.43/0.48

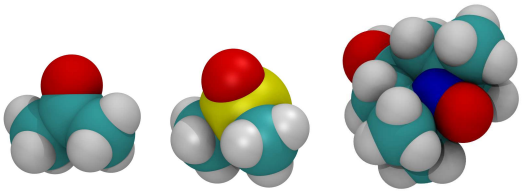

FIG. 1. Molecular structures of acetone (left), DMSO (middle), and TEMPOL (right). Simulation parameters of acetone and DMSO are from Ref. 43, of TEMPOL form Ref. 44. Simulations were performed with NAMD.[45]

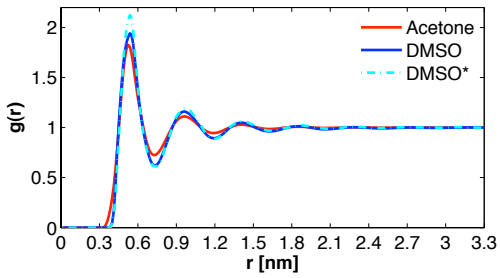

FIG. 2. RDFs between the centers of mass of the solvent molecules from the pure-solvent simulations at 35°C.

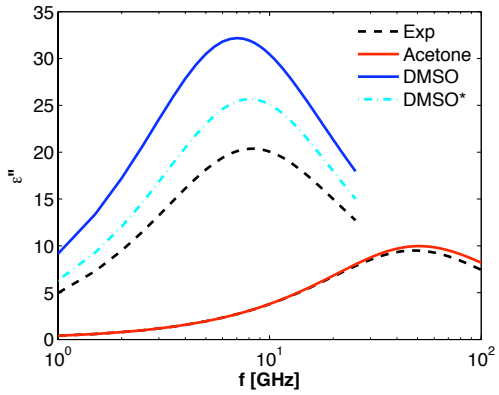

FIG. 3. Imaginary part of the dielectric response function. Experimental data are available up to $\sim$ 25 GHz. For acetone, the analytical fit to experiment at 20°C[25] (dashed line) and our computational prediction for 35°C (red solid line) are extended to 100 GHz to show the peak of the response. MD calculations for the original DMSO model (blue solid line) and the model DMSO* with modified charges (cyan $-\cdot-$) are shown for frequencies probed by experiment[26] (all at 35°C).

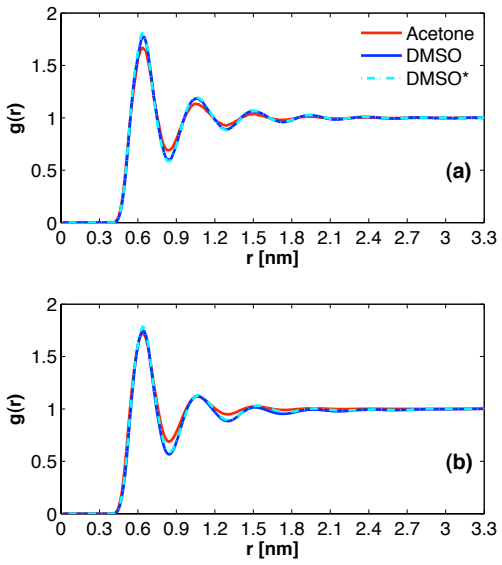

FIG. 4. RDFs between the centers of mass of TEMPOL and the specified solvent molecules from simulations with (a) one TEMPOL molecule and (b) 1 M TEMPOL.

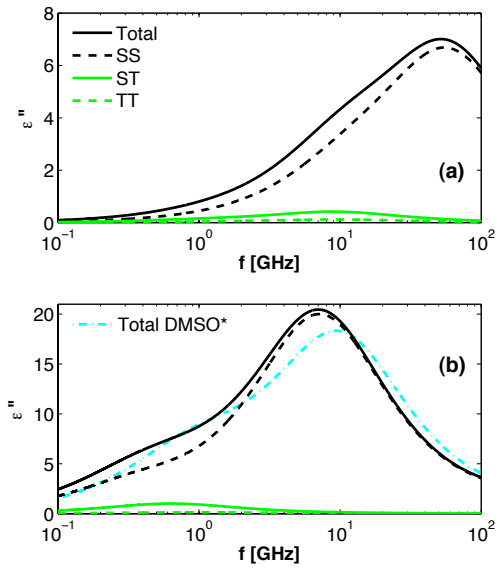

FIG. 5. Dielectric response calculated from the simulations of 1 M TEMPOL in (a) acetone and (b) DMSO.

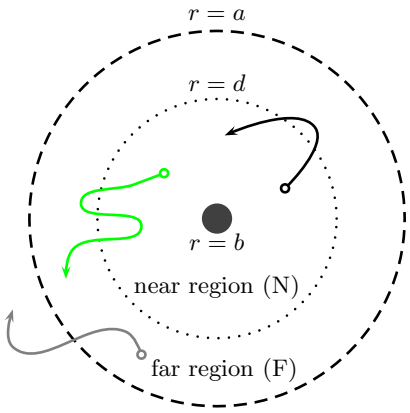

FIG. 6. Definition of near ($r < d$) and far ($d < r < a$) regions around the polarizing agent (sphere of radius b). Trajectories of solvent molecules that are in N at two instances separated by time t (black path) contribute to $C_{\mathrm{NN}}(t)$. Solvent molecules starting in N and moving to F in time t (green path) contribute to $C_{\mathrm{NF}}(t)$. The $r = a$ boundary is assumed to be absorbing. In our analysis, $d = 2.5$ nm and $a = 3.4$ nm.

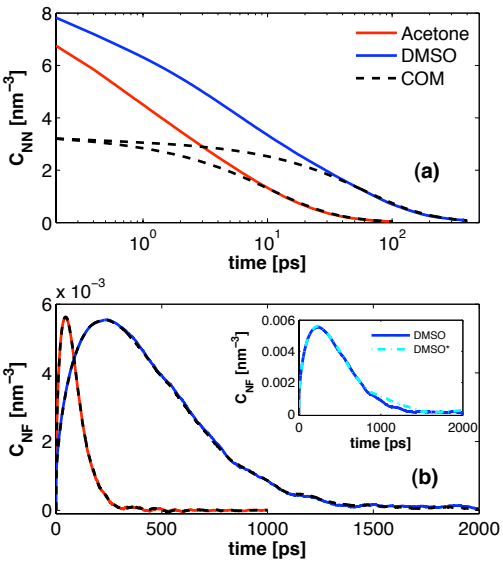

FIG. 7. (a) Near-near and (b) near-far dipolar time correlation functions for acetone (red) and DMSO (blue). Taking the spins to be at the centers of mass (COM) of the molecules (dashed lines) makes a difference in (a) but not in (b). The inset of (b) compares DMSO and DMSO*.

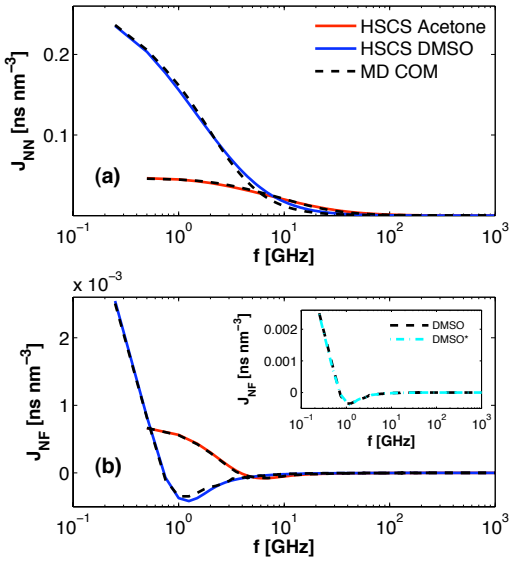

FIG. 8. (a) Near-near and (b) near-far dipolar spectral density functions for acetone (red) and DMSO (blue). Analytical fits with the parameters given in Table 4 (solid lines) agree with MD results for spins assumed to be at molecular COM (dashed lines). The inset of (b) compares DMSO and DMSO*.

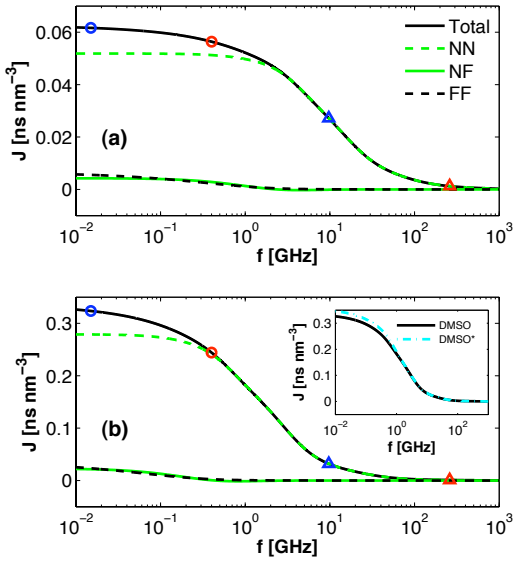

FIG. 9. Dipolar SDF and its additive contributions from the simulations with 1 TEMPOL in acetone (a) and DMSO (b). Symbols indicate SDF values at proton (○) and electron (△) Larmor frequencies at 0.33 T (blue) and 9.2 T (red). The inset of (b) compares the SDFs of DMSO and DMSO*.

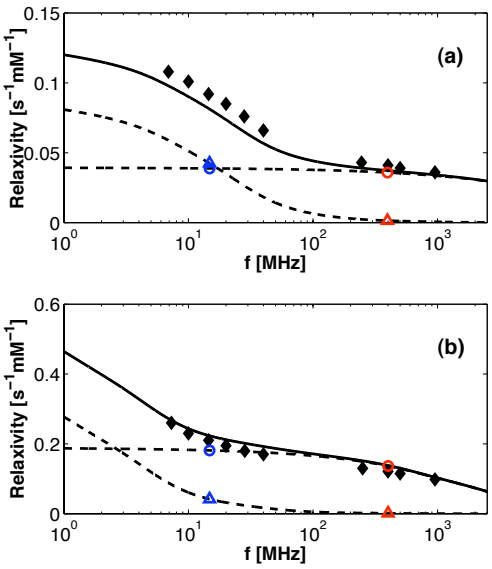

FIG. 10. TEMPOL relaxivities in (a) acetone and (b) DMSO. The relaxivity (solid line) is the sum of two parts proportional to $3J(\omega_I)$ and $7J(\omega_S)$ (dashed lines). Colored $\circ$ and $\triangle$ same as in Fig. 9. Solid diamonds are NMDR values from Ref. 12.

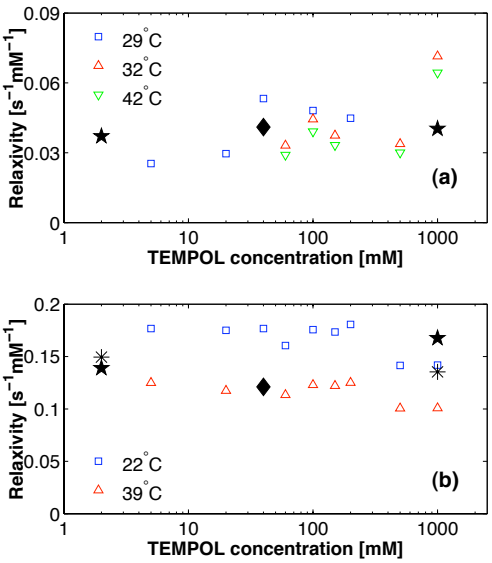

FIG. 11. Relaxivity in (a) acetone and (b) DMSO at 400 MHz. Comparison of estimates from T_1 measurements at 9.2 T for several temperatures and TEMPOL concentrations ($\square$, $\triangle$, $\triangledown$) with values from Ref. 12 ($\blacklozenge$) and computational predictions ($\star$, $*$). The experimental T_1 values are given in SI Table S1.

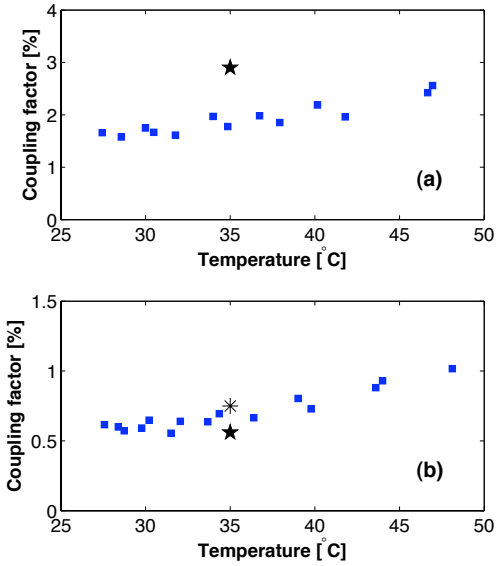

FIG. 12. Coupling factors at 260 GHz for (a) acetone and (b) DMSO. Both experimental (blue squares) and calculated (black stars) values are with 1 M TEMPOL. DMSO* is indicated by asterisk.

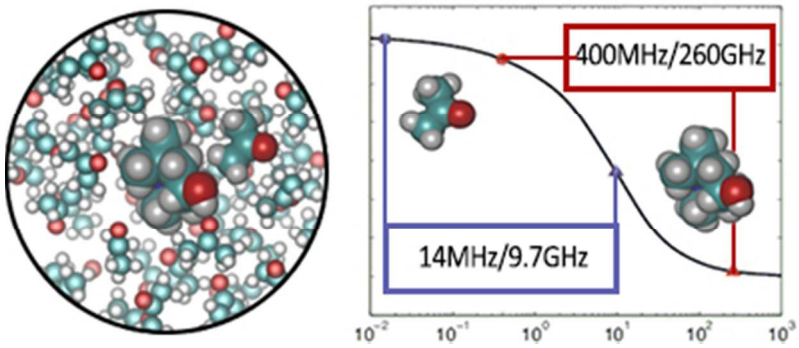

MD simulations enhanced with analytical model of diffusion are used to predict DNP coupling factors.

Molecular simulations for dynamic nuclear polarization in liquids: A case study of TEMPOL in acetone and DMSO

Supporting Information

Sami Emre Küçük,[a] Petr Neugebauer,[b] Thomas F. Prisner,[b] and Deniz Sezer[a]*
[a] *Faculty of Engineering and Natural Sciences, Sabancı University, Orhanlı-Tuzla, 34956 Istanbul, Turkey*
[b] *Institute of Physical and Theoretical Chemistry, Goethe University, Max-von-Laue Str. 7, 60438, Frankfurt am Main, Germany*
(Dated: January 17, 2015)

I. ADDITIONAL RESULTS

A. Analysis of 1 M TEMPOL solutions

The TEMPOL-TEMPOL radial distribution functions (RDFs) calculated from the 1 M TEMPOL simulations are shown in Fig. S1. While the TEMPOL molecules are seen to be well dispersed in acetone and DMSO*, a very small tendency of the radicals to stay closer to each other is seen in the simulation with DMSO.

The near-near (NN) and near-far (NF) contributions to the TEMPOL-solvent dipolar time correlation functions (TCFs) from the 1 M TEMPOL simulations are shown in Fig. S2. The corresponding spectral density functions (SDFs) obtained by Fourier transforming the TCFs are shown in Fig. S3, where the solid lines are analytical fits with the finite-size version[1,2] of the hard-spheres centered-spins (HSCS) model.[3,4]

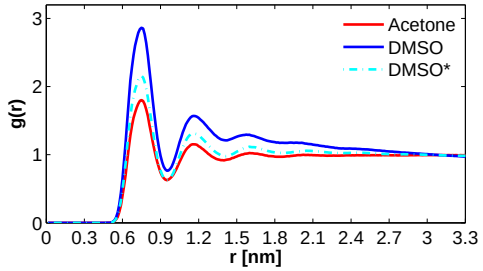

FIG. S1. RDFs between the centers of mass of the TEMPOL molecules in the 1M simulations at 35°C.

The total dipolar SDF and its spatial decomposition are plotted against frequency in Fig. S4.

B. T_1 measurements

Nuclear T_1 values measured for various TEMPOL concentrations, C, are given in Table S1. From these numbers, the relaxivities are calculated as

$$r(C) = \frac{1}{C}\left[\frac{1}{T_1(C)} - \frac{1}{T_1(0)}\right] \qquad \text{(S1)}$$

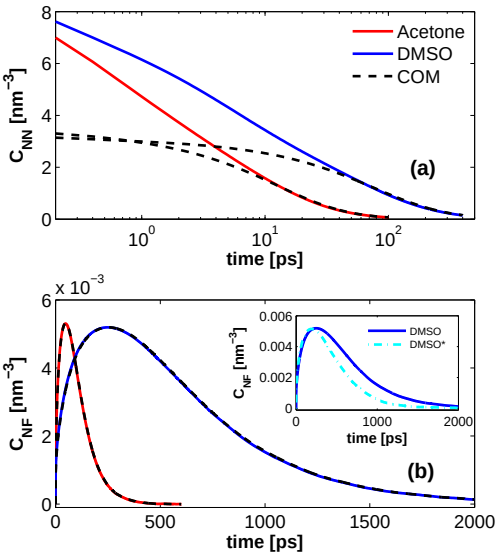

FIG. S2. (a) Near-near and (b) near-far dipolar time correlation functions from the simulations with 1M TEMPOL. Line colors and inset as Fig. 8 of main text.

and reported in Fig. 11 of the main text. In equation (2) of the main text we used the notation $T_1^0 = T_1(0)$ and $T_1^{\mathrm{rad}} = T_1(C)$.

II. METHODS

A. MD simulations

The simulation parameters for acetone and DMSO were from the CHARMM General Force Field (CGenFF),[6] which uses the literature model of DMSO.[7] The atomic partial charges of the modified DMSO model, which we called DMSO*, were taken from Ref. 8. The TEMPOL parameters are from Ref. 9.

All MD simulations were performed with NAMD,[10] accounting for electrostatic interactions with the particle-mesh Ewald method.[11] In all simulations the temperature was kept at 35°C with a Langevin thermostat. Cubic boxes with periodic boundary conditions were used. An

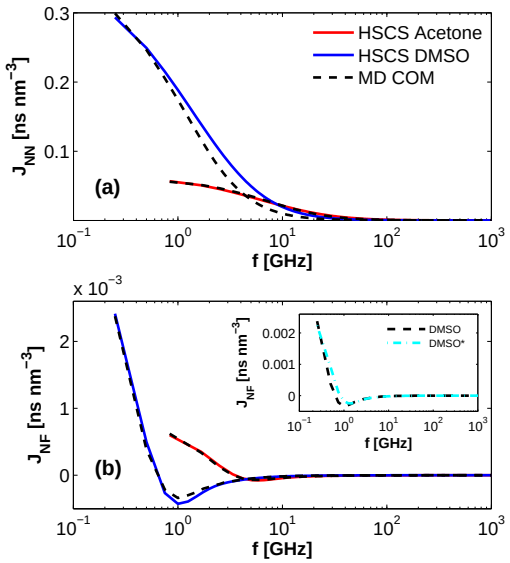

FIG. S3. (a) Near-near and (b) near-far dipolar spectral density functions from the simulations with 1M TEMPOL. Line colors and inset as Fig. 9 of main text.

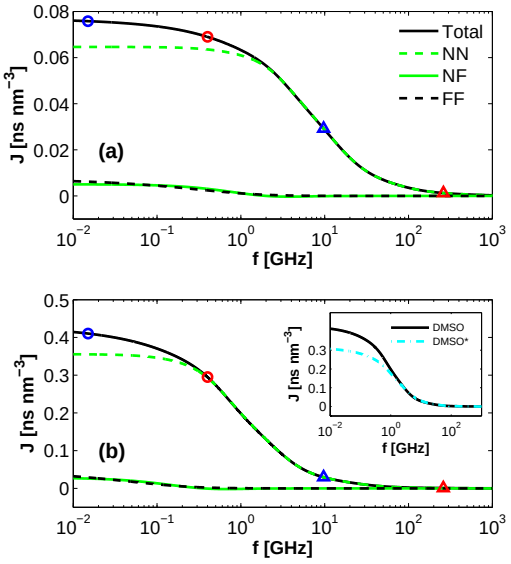

FIG. S4. Dipolar SDF and its additive contributions from the simulations with 1 M TEMPOL in acetone (a) and DMSO (b). Symbols indicate SDF values at proton (○) and electron (△) Larmor frequencies at 0.33 T (blue) and 9.2 T (red). The inset of (b) compares the SDFs of DMSO and DMSO*.

integration time step of 2 fs was employed in conjunction with SETTLE.[12]

First, cubic boxes containing 2744 solvent molecules were created. For each solvent, the size of the simulation box, L, was selected to match the experimental densities of acetone and DMSO at 35°C (Table S2). By carefully choosing the friction coefficients of the Langevin thermostat that maintains the temperature of the MD simulations, we ensured that the diffusion constants of the simulated solutions match the experimental values at 35°C.[13,14] To this end, several constant volume (NVT) simulations were performed for 7 ns with different values of the friction coefficient, γ. The first 1 ns was not analyzed. Diffusion coefficients were estimated from the slope of the mean square displacement in the time interval 400–500 ps. Displacements in the three Cartesian directions were analyzed separately and used to calculate an average and standard deviation. The values of γ for which the average diffusion coefficient was within one standard deviation of the experimental target was selected for the subsequent simulations. These are reported in Table 1 of the main text. The small numerical values of the employed friction (Table 1, main text) indicate that the thermostat does not introduce artificial fast (∼ ps) dynamics.

For simulations with TEMPOL at infinite dilution, 1 TEMPOL molecule was placed into the pure solvent boxes. Four acetone and three DMSO molecules that overlapped with the TEMPOL were removed from the boxes. Constant volume simulations were performed for 11 ns for acetone and 21 ns for DMSO. The first 1 ns was not analyzed (last column of Table S2). Atomic coordinates were saved every 0.2 ps, which is several times less than the electron Larmor frequency at 260 GHz.

For the simulations with high (1 M) TEMPOL concentration, 176 TEMPOL molecules were placed into the pure acetone box and 177 TEMPOL molecules were placed into the pure DMSO box. After removing the

TABLE S1. Nuclear T_1 (in seconds) at 9.2 T for a range of TEMPOL concentrations. These values were used to calculate the relaxivities in Fig. 11 of the main text. The reported temperatures of the samples were deduced as described in Ref. 5.

TEMPOL	acetone			DMSO	
	29.1°C	31.9°C	41.9°C	21.9°C	39.0°C
0 mM	2.751	2.818	3.091	2.539	3.446
5 mM	2.039	-	-	0.783	1.093
20 mM	1.046	-	-	0.257	0.379
40 mM	0.401	-	-	0.134	0.192
60 mM	-	0.427	0.484	0.100	0.141
100 mM	0.193	0.209	0.236	0.056	0.079
150 mM	-	0.168	0.188	0.038	0.054
200 mM	0.1072	-	-	0.027	0.040
500 mM	-	0.058	0.065	0.014	0.020
1000 mM	-	0.014	0.015	0.007	0.010

TABLE S2. Information about the MD simulations of pure solvents or liquids containing 1 TEMPOL.

	ρ/kg m^{-3}	L/nm	T_{pure}/ns	T_{low}/ns
acetone	778	6.9811	1+6	1+10
DMSO/DMSO*	1085	6.8964	1+6	1+20

TABLE S3. Information about the MD simulations with 1 M TEMPOL.

	# TEMPOL+solvent	L/nm	ρ/kg m^{-3}	T_{high}/ns
acetone	176+2048	6.6737	801	5
DMSO	177+2040	6.6689	1063	10
DMSO*	177+2040	6.7127	1042	10

overlapping solvent molecules, 2048 acetone and 2040 DMSO molecules remained (Table S3). Since experimental density information about the 1 M TEMPOL solutions was not available, constant pressure (NPT) simulations were performed for 10 ns to estimate the volume. The average volume of the simulation box over this period was calculated. The box sizes were then fixed by keeping the side lengths at the values given in the third column of Table S3, which imply the densities reported in the fourth column of the same table. After that, constant volume (NVT) simulations were performed for a duration of T_{high} ns.

B. Densities

In order to validate the densities obtained by the computational procedure outlined at the end of the previous paragraph we conducted additional experiments and measured the densities of pure DMSO and of 1 M TEMPOL in DMSO. The density of pure DMSO at 20°C was found to be 1116.64 kg/m^3. Given that the literature value is 1100.53 kg/m^3,[15] our density measurements are seen to be reliable to within 1.5%.

The density of 1 M TEMPOL in DMSO that we measured at 20°C was 1103.18 kg/m^3, which is about 1% lower than our measurement for pure DMSO. Assuming that this relation applies also at 35°C, where we have not performed density measurements, in the MD simulations at this temperature we should observe similar densities for pure DMSO and 1 M TEMPOL in DMSO.

To check this, we simulated pure DMSO (and DMSO*) at 35°C under constant pressure and calculated the average volume. The densities deduced from these simulations are 1078.5 kg/m^3 for DMSO and 1049.9 kg/m^3 for DMSO*. In line with our expectation, both of these values are slightly larger than the densities of the simulated DMSO-TEMPOL solutions reported in Table S3. Thus, the computationally deduced densities of 1 M TEMPOL in DMSO and in DMSO* are reasonable.

Coming back to the simulations of pure DMSO with the two alternative models, DMSO and DMSO*, we note that the MD densities (1078.5 kg/m^3 for DMSO and 1049.9 kg/m^3 for DMSO*) differ from the experimental value at 35°C (1085.24 kg/m^3)[16] by less than 1% and slightly more than 3%, respectively. Clearly, while the modified model DMSO* improves the dielectric relaxation properties of the solvent, it has an adverse effect on the liquid density. This observation is a nice illustration of our claim that the proper development of force-field parameters requires a separate full-blown effort.

C. Dielectric response

The frequency response of the dielectric permittivity is related to the collective electric dipole moment of the entire simulation box with N molecules, expressed as

$$\mathbf{M}(t) = \sum_{a=1}^{N} \mu_a, \tag{S2}$$

where the vector μ_a is the electric dipole moment of molecule a. Let us denote the time correlation functions (TCFs) of the Cartesian components of $\mathbf{M}(t)$ as

$$\Phi_{ij}(t) = \langle M_i(\tau) M_j(\tau + t) \rangle_\tau, \tag{S3}$$

where the angle brackets denote ensemble average and the subscript denotes an additional average over the time variable τ. For a rotationally isotropic system we should have $\Phi_{ij}(t) = \delta_{ij}\Phi(t)$, where δ_{ij} is Kornecker's delta. Thus, $\Phi(t)$ can be estimated by averaging $\Phi_{xx}(t)$, $\Phi_{yy}(t)$ and $\Phi_{zz}(t)$. The standard deviation of the three independent estimates can also be obtained.

The frequency-dependent dielectric constant $\epsilon(\omega)$ is related to the TCF $\Phi(t)$ through the relation[17,18]

$$\epsilon(\omega) = 1 + \frac{1}{V k_{\mathrm{B}} T \epsilon_0} \mathcal{L}[-\dot{\Phi}(t)](\omega), \tag{S4}$$

where V is the volume of the simulation box, $k_{\mathrm{B}}T$ is the thermal energy at temperature T, $\epsilon_0 = 8.85 \times 10^{-12}$ F/m is the permittivity of vacuum, $\dot{\Phi} = \mathrm{d}\Phi/\mathrm{d}t$, and $\mathcal{L}[g]$ is the Fourier-Laplace (or one-sided Fourier) transform of g,

$$\mathcal{L}[g(t)](\omega) = \int_0^\infty g(t) \mathrm{e}^{-\mathrm{i}\omega t} \mathrm{d}t. \tag{S5}$$

We first fit the TCF $\Phi(t)$ obtained from the simulations with a sum of two or three exponential decays,

$$\Phi(t) = \sum_i a_i \mathrm{e}^{-t/\tau_i}, \tag{S6}$$

over the range 0–1 ns. The amplitudes, a_i (Debye squared), and relaxation time scales, τ_i (ps), are given in Table S4 (acetone), Table S5 (DMSO) and Table S6 (DMSO*) for the simulations of pure solvent, dilute (1 TEMPOL) and concentrated (1 M TEMPOL) solutions. From the tables, the dominating timescales are seen to be ~ 3 ps for acetone, 20–25 ps for DMSO, and 15–20 ps for DMSO*. The values vary with the concentration of TEMPOL.

Using the multiexponential fit, we obtain the one-sided Fourier transform

$$\mathcal{L}[-\dot{\Phi}](\omega) = \sum_i \frac{a_i}{1 + \tau_i^2 \omega^2} - \mathrm{i}\omega \sum_i \frac{a_i \tau_i}{1 + \tau_i^2 \omega^2}. \tag{S7}$$

TABLE S4. Multiexponential fitting parameters for acetone.

Pure		1 TEMPOL		1 M TEMPOL	
a_i/D^2	τ_i/ps	a_i/D^2	τ_i/ps	a_i/D^2	τ_i/ps
1273	0.985	332	0.558	582	0.260
22260	3.20	23167	3.07	12709	2.87
				3869	17.2

TABLE S5. Multiexponential fitting parameters for DMSO.

Pure		1 TEMPOL		1 M TEMPOL	
a_i/D^2	τ_i/ps	a_i/D^2	τ_i/ps	a_i/D^2	τ_i/ps
2113	0.398	1505	0.265	2292	0.480
4587	5.46	6683	4.83	40176	22.1
54545	20.8	66415	24.4	6707	394

Thus, for the real and imaginary parts of

$$\epsilon(\omega) = \epsilon'(\omega) - \mathrm{i}\epsilon''(\omega) \tag{S8}$$

we find

$$\epsilon'(\omega) = 1 + \frac{1}{Vk_{\mathrm{B}}T\epsilon_0}\sum_i \frac{a_i}{1+\tau_i^2\omega^2} \tag{S9}$$

and

$$\epsilon''(\omega) = \frac{\omega}{Vk_{\mathrm{B}}T\epsilon_0}\sum_i \frac{a_i\tau_i}{1+\tau_i^2\omega^2}. \tag{S10}$$

Note that the static value of ϵ (reported in Table 1 of main text), which corresponds to $\omega = 0$, is purely real and can be obtained from the initial value of the TCF through the relation:

$$\epsilon = \epsilon'(0) = 1 + \frac{1}{3Vk_{\mathrm{B}}T\epsilon_0}\langle \mathbf{M}(\tau)\cdot\mathbf{M}(\tau)\rangle_\tau. \tag{S11}$$

For a mixture, one can calculate the self- and cross-contributions of the separate components to the TCF and, thus, to $\epsilon(\omega)$. Denoting the electric dipole moments of all the solvent molecules in the simulation box by $\mathbf{M}_{\mathrm{S}}$ and all the TEMPOL molecules by $\mathbf{M}_{\mathrm{T}}$, we have

$$\Phi(t) = \Phi_{\mathrm{SS}}(t) + \Phi_{\mathrm{ST}}(t) + \Phi_{\mathrm{TT}}(t), \tag{S12}$$

where

$$\Phi_{\mathrm{SS}}(t) = \frac{1}{3}\langle \mathbf{M}_{\mathrm{S}}(\tau)\cdot\mathbf{M}_{\mathrm{S}}(t+\tau)\rangle_\tau, \tag{S13}$$

TABLE S6. Multiexponential fitting parameters for DMSO*.

Pure		1 TEMPOL		1 M TEMPOL	
a_i/D^2	τ_i/ps	a_i/D^2	τ_i/ps	a_i/D^2	τ_i/ps
3146	0.859	947	0.146	2358	0.790
56644	19.4	57986	15.9	35888	17.0
1456	64.6	1027	49.1	1315	220

$$\Phi_{\mathrm{TT}}(t) = \frac{1}{3}\langle \mathbf{M}_{\mathrm{T}}(\tau)\cdot\mathbf{M}_{\mathrm{T}}(t+\tau)\rangle_\tau \tag{S14}$$

and

$$\Phi_{\mathrm{ST}}(t) = \frac{2}{3}\langle \mathbf{M}_{\mathrm{S}}(\tau)\cdot\mathbf{M}_{\mathrm{T}}(t+\tau)\rangle_\tau. \tag{S15}$$

Using each of these additive components in (S4) allows us to write

$$\epsilon(\omega) = \epsilon_{\mathrm{SS}}(\omega) + \epsilon_{\mathrm{ST}}(\omega) + \epsilon_{\mathrm{TT}}(\omega), \tag{S16}$$

as claimed in the main text. In practice, separate multi-exponential fits were performed for each of the self- and cross-TCF and used in (S10).

D. Magnetic dipole-dipole coupling

Magnetic dipole-dipole TCFs can be calculated from the coordinates of the spins at two instances τ and $\tau + t$ as follows:

$$C_m(t) = \langle F_m^*(\mathbf{r},\tau)F_m(\mathbf{r},\tau+t)\rangle_\tau. \tag{S17}$$

Here,

$$F_m(\mathbf{r},t) = \frac{Y_2^m(\theta(t),\phi(t))}{r(t)^3}, \tag{S18}$$

Y_2^m's are the rank-2 spherical harmonics, and (r,θ,ϕ) are the spherical coordinates of the vector between the spins, $\mathbf{r}$. In a rotationally isotropic environment, the TCFs are expected to be independent of m. Thus another averaging is performed over $m = -1, 0, 1$ to calculate an m-independent TCF, $C(t)$. The dipolar spectral density function (SDF) is the real part of the Fourier-Laplace transform of the TCF:

$$J(\omega) = \mathrm{Re}\{\mathcal{L}[C(t)](\omega)\}. \tag{S19}$$

The calculation and normalization of near-near and near-far TCFs was performed as described elsewhere.[2] Calculated correlation lengths were 1 ns for acetone and 2 ns for DMSO and DMSO* due to the slower decay rate of the DMSO correlations (*cf.* Fig. 7 in main text). The time resolution of the correlation functions was $\Delta t = 0.2$ ps, which is the frequency with which the coordinates were recorded. This resolution in time limits the frequency bandwidth of the numerical Fourier transform of the TCF to $F = 1/\Delta\mathrm{t}$=5000 GHz. The total duration of the TCF, on the other hand, sets a limit on the frequency resolution. For acetone we had $\Delta f = 0.5$ GHz, whereas for DMSO and DMSO* the resolution was two times higher, $\Delta f = 0.25$ GHz, as reflected by the lowest frequency points in Fig. 8 of the main text.

The near-near TCFs were fit to a sum of decaying exponential functions in order to calculate the SDFs through analytical Fourier transforms, since for

$$C_{\mathrm{NN}}(t) = \sum_{i=1}^{4} a_i \mathrm{e}^{-t/\tau_i} \tag{S20}$$

we have

$$J_{\rm NN}(\omega) = \sum_{i=1}^{4} \frac{a_i \tau_i}{1+\omega^2\tau_i^2}. \qquad \text{(S21)}$$

The intensities and relaxation time scales of the fits are shown in Tables S7 and S8.

TABLE S7. Near-near TCF fitting parameters for liquids with 1 TEMPOL.

Acetone		DMSO		DMSO*	
a_i/nm^3	τ_i/ps	a_i/nm^3	τ_i/ps	a_i/nm^3	τ_i/ps
2.841	0.242	2.801	0.414	2.876	0.395
2.768	1.71	3.237	5.99	3.313	5.62
2.601	9.29	2.768	50.9	2.705	46.1
0.583	36.8	0.469	241	0.730	204

TABLE S8. Near-near TCF fitting parameters for solutions with 1 M TEMPOL.

Acetone		DMSO		DMSO*	
a_i/nm^3	τ_i/ps	a_i/nm^3	τ_i/ps	a_i/nm^3	τ_i/ps
3.087	0.249	2.827	0.419	2.976	0.392
2.738	1.86	2.994	6.45	3.225	5.25
2.642	10.8	2.434	55.4	2.540	42.2
0.658	44.0	0.799	243	0.735	182

The near-near SDFs calculated by assuming that the spins are at the molecular centers of mass (COM) were fit with the finite-size version of the HSCS model. Note that these are only used in the calculation of the finite-size correction $\Delta^{\rm fs}_{\rm NN}$ in Eq. (5) of the main text. The fitting parameters b and D are given in Table 4 of the main text (rows labeled $J_{\rm NN}$).

Although not required by our methodology, one can envision fitting the actual (spins at their correct positions away from the molecular centers) near-near SDFs with the finite-size version of the HSCS model. Such fits are depicted in Fig. S5. The fitting parameters are $b = 0.38$ nm, $D = 5.95$ nm^2/ns for acetone, and $b = 0.40$ nm, $D = 1.03$ nm^2/ns for DMSO. Clearly, they are different from the values reported in the last three rows of Table 4 of the main text. The fits in Fig. S5, however, seem to be comparable in quality to the ones for the near-near SDFs calculated by assuming that the spins are at the molecular COM and shown in Fig. 8a of the main text.

If the finite-size version of the HSCS model fits the actual near-near SDFs, why do we use multiexponential fits to the near-near TCFs [*cf.* Eq. (S20)]? Even more importantly, how can a model assuming centered spins fit the SDFs of off-centered spins? To investigate this point, the plots in Fig. 8a and Fig. S5 are reproduced in Fig. S6 with logarithmic scales on both the vertical and horizontal axes. We observe that the near-near SDFs calculated from the MD simulations by assuming that

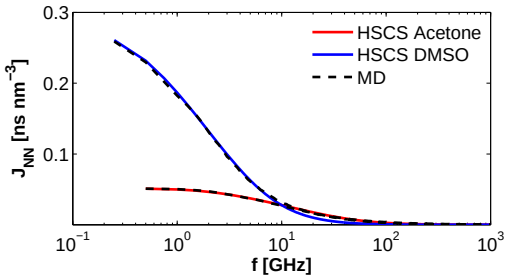

FIG. S5. Near-near SDFs calculated from the MD simulations for spins at their actual positions (dashed lines) and best fits with the finite-size HSCS model (solid lines).

the spins are at the centers of the molecules (dashed lines in Fig. S6a) agree well with the analytical model (solid lines) over the whole frequency range. In contrast, the near-near SDFs calculated from the MD simulations by using the actual positions of the spins (dashed lines in Fig. S6b) deviate substantially from the predictions of the HSCS model at the higher frequencies shown in the figure. In Fig. S6b the slopes of the analytical lines at high frequencies are very different than the slopes of the MD lines. This confirms our expectation that at short spin-spin distances, as is the case in the near region, the HSCS model should fail to fit the actual near-near SDF. A multiexponential fit does an excellent job at fitting the MD lines in Fig. S6b (not shown).

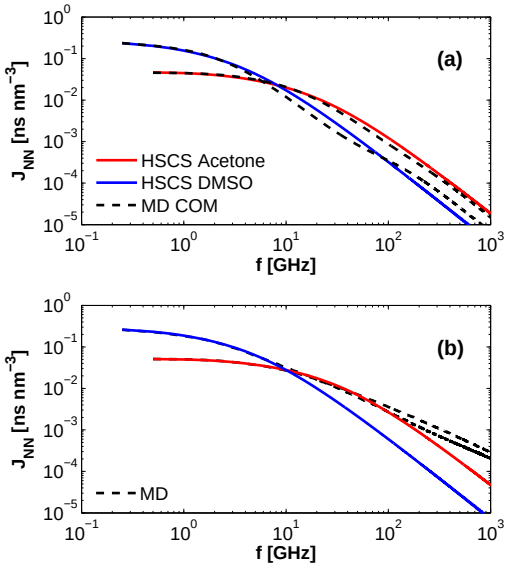

FIG. S6. (a) Same as Fig. 8a in main text with logarithmic vertical axis. (b) Same as Fig. S5 with logarithmic vertical axis.

* dsezer@sabanciuniv.edu

[1] B. Halle, J. Chem. Phys. **119**, 12373 (2003).
[2] D. Sezer, Phys. Chem. Chem. Phys. **15**, 526 (2013).
[3] Y. Ayant, E. Belorizky, J. Alizon, and J. Gallice, J. Phys. (Paris) **36**, 991 (1975).
[4] L.-P. Hwang and J. H. Freed, J. Chem. Phys. **63**, 4017 (1975).
[5] P. Neugebauer, J. G. Krummenacker, V. P. Denysenkov, C. Helmling, C. Luchinat, G. Parigi, and T. F. Prisner, Phys. Chem. Chem. Phys. **16**, 18781 (2014).
[6] K. Vanommeslaeghe, E. Hatcher, C. Acharya, S. Kundu, S. Zhong, J. Shim, E. Darian, O. Guvench, P. Lopes, I. Vorobyov, and A. D. Mackerell, J. Comput. Chem. **31**, 671 (2010).
[7] M. L. Strader and S. E. Feller, J. Phys. Chem. A **106**, 1074 (2002).
[8] P. Bordat, J. Sacristan, D. Reith, S. Girard, A. Glättli, and F. Müller-Plathe, Chem. Phys. Lett. **374**, 201 (2003).
[9] D. Sezer, J. H. Freed, and B. Roux, J. Phys. Chem. B **112**, 5755 (2008).
[10] J. C. Phillips, R. Braun, W. Wang, J. Gumbart, E. Tajkorshid, E. Villa, C. Chipot, R. D. Skeel, L. Kale, and K. Schulten, J. Comp. Chem. **26**, 1781 (2005).
[11] U. Essmann, L. Perera, M. L. Berkowitz, T. Darden, H. Lee, and L. G. Pedersen, J. Chem. Phys. **103**, 8577 (1995).
[12] S. Miyamoto and P. A. Kollman, J. Comp. Chem. **13**, 952 (1992).
[13] H. Ertl and F. A. L. Dullien, AIChE Journal **19**, 1215 (1973).
[14] M. Holz, S. R. Heil, and A. Sacco, Phys. Chem. Chem. Phys. **2**, 4740 (2000).
[15] N. G. Tsierkezos, A. E. Kelarakis, and M. M. Palaiologou, J. Chem. Eng. Data **45**, 395 (2000).
[16] U. R. Kapadi, S. K. Chavan, and O. S. Yemul, J. Chem. Eng. Data **42**, 548 (1997).
[17] C. J. F. Böttcher and P. Bordewijk, *Theory of Electric Polarization*, 2nd ed., Vol. II: Dielectrics in Time-Dependent Fields (Elsevier Science B. V., 1978).
[18] S. Gekle and R. R. Netz, J. Chem. Phys. **137**, 104704 (2012).